Use of Log-Normal Distributions for Numerical Calculations of Condensation and Collection

TERRY L. CLARK

Atmospheric Environment Service, Downsview, Ontario, Canada

(Manuscript received 15 November 1974, in revised form 23 January 1976)

ABSTRACT

Lagrangian parcel calculations of condensation and coalescence theory are presented where both a distribution function approach as well as a conventional finite-difference approach are compared. The comparisons suggest that the use of series of log-normal distributions to represent the water droplet spectra may be a practical approach to treating cloud physical processes in multi-dimensioned cloud models.

1. Introduction

This paper presents some Lagrangian parcel-type calculations on the cloud physical equations of condensation and coalescence theory using series of distribution functions. The main purpose of this research was to develop a methodology for the inclusion of the various microphysical processes into multi-dimensioned cloud models. Ideally one would like a method which requires little computer storage area and little computer central processing time while maintaining a reasonable degree of accuracy in the results. The accuracy, speed, and field-variable storage requirements of the present method are all discussed. The accuracy is assessed by a comparison of results, for the somewhat academic cases treated, between a conventional finite-difference model and the present model. The finite-difference model is run for various grid-spacing resolutions where the maximum number of grid points used for these comparison tests was 181.

A lot of research has been done on investigating analytical solutions of the stochastic coalescence equations where the collection kernel has been approximated in some relatively simple analytical form. Typically these investigations use the method of moments where a recursion formula for any moment tendency is required in a closed form. For the general case of any collection kernel, as discussed by Drake (1972), closed equations for the moments cannot be obtained. This seems to be one of the strong limitations of this approach for the results to be used in microphysical cloud models. I refer the reader to the more recent papers of Long (1974) and Drake (1972) for a more detailed discussion of the work in this area. The purpose of the present research is similar to that of the earlier work mentioned, except that the present approach taken is somewhat different. Instead of looking for closed forms of equations in distribution moment space, closure is forced on the system through the assumption that the droplet- and drop-distribution functions remain self-similar for all time. The self-similarity parameters in this case are not arrived at through careful analysis, but are prescribed as being the parameters of two or more distribution functions. This empirical assumption will only lead to approximate time-dependent solutions of the microphysical equations. One aspect of this paper is to investigate the degree of accuracy when two log-normal or two gamma distributions are used to represent the evolving distribution when condensation and stochastic coalescence theory are treated.

One advantage of this approach is that it does not require the collection kernel to take on any particular analytical form. In fact, as in the examples treated, the non-analytical, geometric, sweep-out kernel form is assumed. By assuming that the total moment tendencies in radius space up to a certain order contain enough information to give a fairly accurate solution, the method is easily applied to more than one physical process at a time. The two main questions with respect to this approach are: does the method allow for reasonably accurate solutions?, and, does the arbitrary moment closure assumption allow for numerical stability? This paper only treats one set of initial conditions for a particular form of condensation particle growth and for the geometric sweep-out collection kernel. Thus the results of this investigation can only be considered as encouraging evidence that the scheme is an appropriate one for consideration in Lagrangian, as well as dynamical, models.

2. Governing equations of the model

The model to be described treats the physical processes of coalescence and condensation theory in a Lagrangian parcel sense. The dynamics is crudely

treated by assuming a constant vertical velocity w of 2 m s^{-1} (for all runs) and a constant eddy-mixing coefficient K, where the magnitude of K depends on the particular run. The microphysical processes are treated using the kinetic equation

$$\frac{df}{dt}=-\frac{\partial}{\partial r}\left(f\frac{dr}{dt}\right)+\text{COAL}+\text{DIFF}, \tag{2.1}$$

where the density function $f(r)$ describes the number of drops per cubic centimeter between radii r to $r+dr$. The first term on the right-hand side of (2.1) represents the spectral spreading and shifting effects of droplet growth due to the condensation of water vapor onto existing droplets.

The diffusional growth rate for a droplet of radius r is assumed to take the form

$$\frac{dr}{dt}=\frac{kS}{r+l}, \tag{2.2}$$

where S is the supersaturation. The value of 0.033 for the condensation coefficient, as well as the formulation of k and l, are taken from Chodes *et al.* (1974). The second term on the right-hand side of (2.1), COAL, represents the effects of "quasi-stochastic" coalescence theory where, following Berry (1967), the contribution to the tendency of f in terms of drop mass is given as

$$\text{COAL}=\int_0^{m/2} f(m-m')f(m')V(m-m'|m')dm' - \int_0^{\infty} f(m)f(m')V(m|m')dm'. \tag{2.3}$$

The collection kernel $V(m|m')$ is taken as the geometric sweep-out kernel, i.e.,

$$V(r|r')=\pi(r+r')^2|V_T(r)-V_T(r')|, \tag{2.4}$$

where V_T represents the drops terminal velocity. The reason for choosing this somewhat unrealistic kernel is that a relatively strong coalescence forcing was desired for both economical as well as mathematical purposes. Shorter time intervals are required for substantial cloud development to occur and resolution experiments with conventional finite-difference methods become more economical. Also, since a new mathematical technique for solving the equations is being tested, strong forcing in the equations is likely to demonstrate where the problem areas are in the methodology. (This was certainly found to be the case.) Geometric sweep-out is the strongest forcing likely to be considered in a cloud model calculation. The third term on the right-hand side of (2.1), DIFF, crudely represents the effects of stochastic condensation theory. Sedunov (1974) derives this term as

$$\frac{df}{dt}=\frac{1}{\beta}\left(\frac{\partial}{\partial z}+\beta\frac{\partial}{\partial r}\right)K\left(\frac{\partial}{\partial z}+\beta\frac{\partial}{\partial r}\right)\beta f, \tag{2.5}$$

where

$$\beta=\frac{kS_q}{w(r+l)}, \tag{2.6}$$

and S_q is the quasi-steady value of S. The physical assumptions leading to (2.5) are that S and its deviations S' are approximately equal to S_q and S_q', respectively. These assumptions imply that sufficient numbers of droplets exist such that the time scale of response of the droplet field to changes in the S field are much smaller than the time scale of the change of S. As stated by Sedunov (1974), these assumptions are not applicable to the cloud base region and thus different physical assumptions seem necessary to treat this area. If one takes the opposite extreme and assumes that the time scale of the change of S, due to turbulent fluctuations, is much smaller than the time scale of response of the droplet field, then one can assume that essentially no droplet growth occurs during the mixing of parcels. In this case we consider $f(r)$ a conservative quantity during mixing, and the Prandtl mixing length hypothesis leads to

$$\frac{df}{dt}=\frac{\partial}{\partial z}\left(K\frac{\partial f}{\partial z}\right). \tag{2.7}$$

In order to eliminate the spatial coordinate from (2.7) some further simplifying assumptions need to be made. The assumptions that the turbulent mixing causes a small perturbation on the mean value of $f(r)$ and that the distribution of f with height is steady state allow the vertical derivative to be approximated as

$$w\frac{\partial f}{\partial z}=-\frac{\partial}{\partial r}\left(f\frac{dr}{dt}\right). \tag{2.8}$$

Here we are considering mixing of the smaller particles where their rapid variation with height is mainly due to condensation theory. Substitution of (2.8) into (2.7) gives us the presently used formulation of DIFF:

$$\text{DIFF}=K\left(\frac{kS}{w}\right)^2\frac{\partial}{\partial r}\left[\frac{\partial}{r+l}\frac{1}{\partial r}\left(\frac{f}{r+l}\right)\right]. \tag{2.9}$$

Incorporation of (2.9) into a Lagrangian parcel model allows one to study the effects of mixing on the evolution of the droplet distribution with a minimum of expense. The limiting effects of the model assumptions must be carefully considered when interpreting the results.

The thermodynamic system of equations includes the S equation

$$\frac{dS}{dt}=T_S w-H_2C_d, \tag{2.10}$$

where

$$C_d=4\pi\frac{\rho_l}{\rho_a}\int_0^\infty r^2 f\langle r\rangle\frac{dr}{dt}dr, \tag{2.11}$$

$$H_2=\frac{1}{q_{vs}}\left(1+\frac{L^2q_v}{R_vC_pT^2}\right), \tag{2.12}$$

$$T_S=(1+S)\frac{g}{R_dT}\left(\frac{\epsilon L}{C_pT}-1\right), \tag{2.13}$$

$$S=(q_v/q_{vs})-1. \tag{2.14}$$

The saturation value of the water vapor mixing ratio, q_{vs}, is taken as

$$q_{vs}=\frac{\epsilon e_0}{P}\exp\left[\frac{L(T-T_0)}{R_vTT_0}\right], \tag{2.15}$$

where $e_0=6.11$ mb and $T_0=273.16$ K. The remaining equations are the conservation equation for water vapor mixing ratio

$$\frac{dq_v}{dt}=-C_d, \tag{2.16}$$

and the tendency equations for temperature T and pressure P

$$\frac{dT}{dt}=(-wg+LC_d)/C_p, \tag{2.17}$$

$$\frac{dP}{dt}=-\rho_a wg. \tag{2.18}$$

The thermodynamic system is redundant in that the supersaturation is treated twice, once in (2.10) and once in (2.14)–(2.18). The model calculations were checked to insure that there were no serious inconsistencies between the two calculations of S. This subject is discussed in more detail by Clark (1973).

The system of equations (2.1)–(2.4) and (2.9)–(2.18) will be solved using two types of numerical models. The first model is a conventional finite-difference model designed with variable resolution in the radius domain. This model will be run for various resolutions until an acceptable level of convergence has been obtained. The second model will use series of distribution functions to represent the structure of the evolving water spectrum. The results of these calculations will be compared with the "converged" solution of the finite-difference model. The next section will discuss the numerical methods used for the finite-difference model.

3. Numerical methods for the finite-difference model

The stochastic coalescence terms of the kinetic equation are solved using the methods of Berry (1967) and Berry and Reinhardt (1974). The distribution density function is transformed to J space where

$$r_J=r_0 2^{(J-1)/(3JRS)}, \tag{3.1}$$

for $JRS=2, 3, 4, 5, 6$. The transformation is

$$f\langle r\rangle dr=f\langle J\rangle dJ, \tag{3.2}$$

$$f\langle r\rangle=f\langle J\rangle\frac{dJ}{dr}=\frac{3(JRS)}{\ln 2}\frac{1}{r}f\langle J\rangle, \tag{3.3}$$

and the integral-differential equations become

$$\frac{df}{dt}\langle J\rangle=\int_1^{JD}\frac{f\langle JP\rangle f\langle JC\rangle}{(1-r_{JP}^3/r_J^3)}V(JP|JC)d(JP)$$

$$-\int_1^\infty f\langle J\rangle f\langle JP\rangle V(J|JP)d(JP), \tag{3.4}$$

where

$$\left.\begin{aligned}JD&=J-JRS\\ m_J&=m_{JC}+m_{JP}\end{aligned}\right\}. \tag{3.5}$$

The method of determining $f\langle JC\rangle$ was by a 6-point Lagrangian interpolation scheme where the interpolation was performed on the logarithms of $f\langle J\rangle$. The accuracy of this interpolation is very important to the accuracy of the coalescence calculation as pointed out by Berry and Reinhardt (1974). The integrations were performed using 3, 4 and 5 point schemes as described by Berry (1967). Forward time steps with $\Delta t=0.25$ s were used. The values chosen for radius were

$$r_0=0.25\ \mu\text{m} \tag{3.6}$$

in all radius resolution cases and J was incremented such that

$$r_{\max}=256\ \mu\text{m}. \tag{3.7}$$

Thus, these experiments describe only the initiation of rain formation. The number of grid increments used was 61, 91, ..., 181 for $JRS=2, 3, \ldots, 6$, respectively.

The finite differencing for the "stochastic" condensation terms were also performed on $f\langle J\rangle$ and the transformed equation becomes

$$\frac{\partial}{\partial t}f\langle J\rangle=-\frac{\partial}{\partial J}\left(f\langle J\rangle\frac{dJ}{dt}\right)+\eta'\frac{\partial}{\partial J}$$

$$\times\left[\frac{1}{r(r+l)}\frac{\partial}{\partial J}\left(\frac{f\langle J\rangle}{r(r+l)}\right)\right], \tag{3.8}$$

where

$$\eta'=K\left(\frac{kS}{w}\right)^2\left(\frac{3JRS}{\ln 2}\right)^2. \tag{3.9}$$

A slightly unstable numerical procedure was used with the instability being eliminated by a procedure which can be termed "hole-filling." Using Schuman operators,

the finite difference analog to (3.8) is

$$\delta_t f = -\delta_J\left(\bar{f}^J\frac{dJ}{dt}-F\right), \tag{3.10}$$

where

$$F_{J+\frac{1}{2}}=\frac{\eta'}{r_{J+\frac{1}{2}}(r_{J+\frac{1}{2}}+l)}\delta_J\left(\frac{f}{r(r+l)}\right). \tag{3.11}$$

The operator on an arbitrary variable ϕ is given as

$$\left.\begin{aligned}\bar{\phi}^J&=[\phi(J+\tfrac{1}{2})+\phi(J-\tfrac{1}{2})]/2\\ \delta_J\phi&=[\phi(J+\tfrac{1}{2})-\phi(J-\tfrac{1}{2})]\\ \delta_t\phi&=[\phi(t+\Delta t)-\phi(t)]/\Delta t\end{aligned}\right\}. \tag{3.12}$$

Forward time steps with $\Delta t=0.25$ s were again used.

The hole-filling scheme used was a number-conservative scheme where any negative number concentrations were eliminated by subtracting from the neighbor which had "too large" an influx. This acts as a slight numerical dispersion but guarantees positive definiteness to $f\langle J\rangle$ and thus also guarantees stability. The dispersive effect of this approach is minimal, whereas the alternative numerical schemes are either expensive or excessively dispersive.

The next section will describe the method of using distribution functions to solve the system of equations.

4. Distribution model description

Two types of distribution functions are used in this study: the gamma distribution which is given as

$$f\langle r\rangle=\frac{N\alpha^\alpha}{\Gamma(\alpha)\bar{R}}\left(\frac{r}{\bar{R}}\right)^{\alpha-1}\exp(-\alpha r/\bar{R}), \tag{4.1}$$

where α is the shape parameter, and N and $\bar{R}$ the distribution number concentration and mean radius, respectively; the log-normal distribution is given as

$$f\langle r\rangle=\frac{N}{\sqrt{2\pi}\sigma r}\exp[-(\ln r-\mu)^2/(2\sigma^2)], \tag{4.2}$$

where μ and σ^2 are the mean and variance of $\ln r$, respectively. Some basic recursion formuli for the distribution moments are

$$\overline{R_i^P}=[1+(p-1)/\alpha_i]\overline{R_i^{P-1}}\,\overline{R_i} \tag{4.3}$$

$$\overline{R_i^P}=\exp(p\mu_i+\tfrac{1}{2}p^2\sigma_i^2), \tag{4.4}$$

for the gamma and log-normal set, respectively. The subscript i refers to the ith distribution of a set of either two or more distributions. The integral definition of $\overline{R_i^P}$ is

$$N_i\overline{R_i^P}=\int_0^\infty r^P f_i\langle r\rangle dr, \tag{4.5}$$

where p is assumed to be an integer.

The approach adopted for using series of distributions is to first calculate a set of total moment tendencies given by the column matrix $\mathbf{F}$, where the transpose of $\mathbf{F}$ is given as

$$\mathbf{F}^T=\left[\frac{d\ln N}{dt},\frac{d\ln N\bar{R}}{dt},\ldots,\frac{d\ln N\overline{R^{\nu-1}}}{dt}\right], \tag{4.6}$$

where $I=\nu/3$ is the number of distributions used. The total moment $\overline{NR^P}$, is then defined as

$$\overline{NR^P}=\sum_{i=1}^{I}N_i\overline{R_i^P}. \tag{4.7}$$

The determination of the matrix components of (4.6) is one of the main aspects of this theory and this subject will be dealt with later. Assuming we have calculated $\mathbf{F}$ we can then write a matrix equation

$$\mathbf{A}\mathbf{X}=\mathbf{F}, \tag{4.8}$$

where $\mathbf{A}$ is a matrix of order ν and the transpose of $\mathbf{X}$, $\mathbf{X}^T$, is given as

$$\mathbf{X}^T=\left[\frac{d\ln N_1}{dt},\frac{d\ln N_2}{dt},\ldots,\frac{d\ln N_I}{dt},\frac{d\mu_1}{dt},\ldots,\frac{d\sigma_1^2}{dt},\ldots,\frac{d\sigma_I^2}{dt}\right]. \tag{4.9}$$

Using relations (4.3), (4.4) and (4.6)–(4.9), we find that the matrix elements a_{ij} of $\mathbf{A}$ are given as

$$\left.\begin{aligned}a_{ij}&=N_j\overline{R_j^{i-1}}/(N\overline{R^{i-1}})\\ a_{ij+I}&=(i-1)N_j\overline{R_j^{i-1}}/(N\overline{R^{i-1}})\\ a_{ij+2I}&=\tfrac{1}{2}(i-1)^2t_{ij}N_j\overline{R_j^{i-1}}/(N\overline{R^{i-1}})\end{aligned}\right\}, \tag{4.10}$$

where $i=1, 2, \ldots, \nu$ and $j=1, 2, \ldots, I$. The matrix $\mathbb{T}$ which has elements t_{ij} has all of its elements equal to unity for a log-normal set, whereas for the gamma distribution set we have

$$t_{ij}=\begin{cases}1, & \text{for } i=2, \text{ all } j\\ \dfrac{1}{(i-1)}+\dfrac{2}{(i-1)^2}(1+1/\alpha_j)\displaystyle\sum_{s=1}^{i-2}\frac{s}{(1+s/\alpha_j)}, & \\ & \text{for } i=3, 4, \ldots, \text{and all } j.\end{cases} \tag{4.11}$$

Once we have calculated the elements of $\mathbb{F}$ and $\mathbb{A}$ we can then proceed to solve (4.8) and subsequently update the three parameters of each distribution function. In this manner we carry out the time integration of the cloud physical equations.

The method as it has been outlined has been found to be numerically stable as long as the total moment tendencies are calculated in a sense which is both consistent with the type of distribution function being

used, as well as relatively free from random errors. The major portion of the research leading to the present results was involved with the elimination of a numerical instability caused by the "noise" of $\mathbf{A}^{-1}$ correlating with noise in $\mathbf{F}$. Once $\mathbf{F}$ was calculated in a sense such that random fluctuations were eliminated, the noisy character of $\mathbf{A}^{-1}$ no longer caused problems. The next sections will describe the methods used to calculate $\mathbf{F}$ where some of the essential detail is discussed.

5. Calculation of condensation total moment tendencies

The condensation process considers an equation of the form

$$\frac{df}{dt}=-\frac{\partial}{\partial r}\left(\frac{fkS}{r+l}\right)+\eta\frac{\partial}{\partial r}\left[\frac{1}{r+l}\frac{\partial}{\partial r}\left(\frac{f}{r+l}\right)\right], \quad (5.1)$$

where

$$\eta=K\left(\frac{kS}{w}\right)^2. \quad (5.2)$$

Multiplication of (5.1) by r^p and integration from $r=0$ to ∞ leads to

$$\frac{d\overline{NR^p}}{dt}=pkS\chi_1^{p-1}+p(p-1)\eta\chi_2^{p-2}-p\eta\chi_3^{p-1}, \quad (5.3)$$

where

$$\chi_n^p=\int_0^\infty \frac{r^p f(r)dr}{(r+l)^n}. \quad (5.4)$$

Once the lowest order values of χ_n^p have been numerically calculated, the recursion formulas

$$\chi_1^p=\overline{NR^{p-1}}-l\chi_1^{p-1}, \qquad p=1, 2, \ldots, \quad (5.5)$$

$$\chi_2^p=\overline{NR^{p-2}}-2l\chi_2^{p-1}-l^2\chi_2^{p-2}, \qquad p=2, 3, \ldots, \quad (5.6)$$

$$\chi_3^p=\overline{NR^{p-3}}-3l\chi_3^{p-1}-3l^2\chi_3^{p-2}-l^3\chi_3^{p-3}, \qquad p=3, 4, \ldots, \quad (5.7)$$

are used to calculate the higher order terms. Thus the main computational effort is in the calculation of χ_1^0, χ_2^0, χ_2^1, χ_3^0, χ_3^1 and χ_3^2. (Only χ_1^0 is required if we let $K=0$.) In order to calculate these parameters each distribution function is broken into a number of finite categories and the χ_n^p functions are calculated using a three-point integration scheme for the gamma distribution set and an eighth-order Lagrangian polynonial scheme for the log-normal set.

TABLE 1. Description of cases treated with both the distribution models as well as the finite-difference models.

Case	Distributions used	Eddy mixing	Other physics treated
1	Two log-normals	$K=0$	Condensation only
2	Two log-normals	$K=0$	Condensation plus coalescence
3	Two log-normals	$K=4$ m^2 s^{-1}	Condensation plus coalescence
4	Two gammas	$K=4$ m^2 s^{-1}	Condensation only

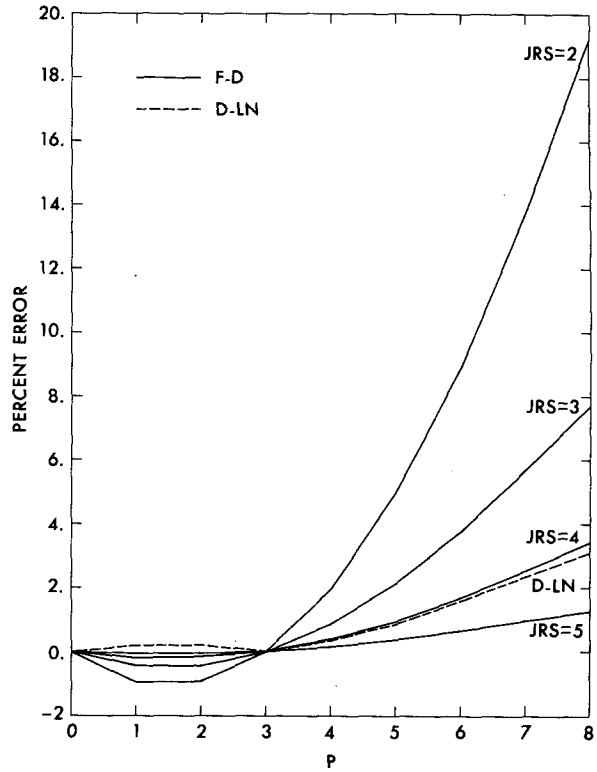

FIG. 1. Comparison of total moment errors at $t=500$ s for case 1. The percent error is taken relative to the F-D ($JRS=6$) calculation. The moment number p is defined through Eqs. (4.5) and (4.7).

The 25 radii values of

$$r_k=\begin{cases}\bar{R}_i\exp\left[\dfrac{k-16}{2(\alpha_i-3)^{\frac{1}{2}}}\right], & \text{for } \alpha_i\geq 4\\[2ex] \bar{R}_i\exp\left[\dfrac{k-16}{(\alpha_i)^{\frac{1}{2}}}\right], & \text{for } \alpha_i<4\end{cases} \quad (5.8)$$

for $k=1, \ldots, 25$ were found to give reasonably accurate results for the calculations of χ_n^p for the gamma distribution case. The symmetry properties of the log-normal distributions about μ_i permit the easy and economical approximate integration of integrals such as χ_n^p via high-order Lagrangian polynomial fits of that portion of the integrand multiplying the distribution function. Consider the arbitrary integral Λ, where

$$\Lambda=\int_{-\infty}^{+\infty}\gamma f_i(\ln r)d\ln r, \quad (5.9)$$

for the ith log-normal distribution. Letting

$$x_i=(\ln r-\mu_i)/(\sqrt{2}\sigma_i), \quad (5.10)$$

Λ becomes

$$\Lambda=\frac{N_i}{\sqrt{\pi}}\int_{-\infty}^{+\infty}\gamma(x)e^{-x^2}dx. \tag{5.11}$$

Then fitting $\gamma(x)$ to the nine points

$$x_k=(k-5)\Delta, \tag{5.12}$$

for say $\Delta=0.58$, the approximate solution of (5.11) becomes

$$\Lambda=N_i\Big[\sum_{k=1}^{4}WG_k(\gamma_k+\gamma_{10-k})+WG_5\gamma_5\Big], \tag{5.13}$$

where the five weighting factors, WG_k, have been previously calculated and permanently stored. This approach to integration for the log-normal set is extremely simple to set up and has been found to be reasonably economical and accurate. The methods of determining WG_k are well known but since the integration method just outlined is also being used in the next section for the determination of tendencies in stochastic coalescence theory it might be useful to present the generating formuli for WG_k for the readers' easy reference. They were calculated to be

$$WG_1=\left\{-9+\frac{1}{\Delta^2}\left[18.375+\frac{1}{\Delta^2}\times\left(-13.125+\frac{3.28125}{\Delta^2}\right)\right]\right\}\Big/(20160\Delta^2),$$

$$WG_2=\left\{128+\frac{1}{\Delta^2}\left[-252+\frac{1}{\Delta^2}\times\left(157.5-\frac{26.25}{\Delta^2}\right)\right]\right\}\Big/(20160\Delta^2),$$

$$WG_3=\left\{-1008+\frac{1}{\Delta^2}\left[1774.5+\frac{1}{\Delta^2}\times\left(-682.5+\frac{91.875}{\Delta^2}\right)\right]\right\}\Big/(20160\Delta^2),$$

$$WG_4=\left\{8064+\frac{1}{\Delta^2}\left[-5124+\frac{1}{\Delta^2}\times\left(1522.5-\frac{183.75}{\Delta^2}\right)\right]\right\}\Big/(20160\Delta^2),$$

$$WG_5=1-2\sum_{k=1}^{4}WG_k,$$

for an eighth-order Lagrangian fit of $\gamma(x)$ to the nine points given by (5.12). Due to the elimination of all odd powers of x in the expansion of $\gamma(x)$ we have

$$WG_{10-k}=WG_k,$$

which leads to the form of Λ given in (5.13).

6. Calculation of the coalescence total moment tendencies

The stochastic coalescence equations (2.3) are recast in the form (Thompson, 1968)

$$\frac{d}{dt}N\overline{R^p}=\tfrac{1}{2}\int_0^\infty\int_0^\infty F^p(r_1,r_2)V(r_1|r_2)\times f\langle r_1\rangle f\langle r_2\rangle dr_1dr_2, \tag{6.1}$$

where

$$F^p(r_1,r_2)=[(r_1^3+r_2^3)^{p/3}-r_1^p-r_2^p], \tag{6.2}$$

$$V(r_1|r_2)=\pi(r_1+r_2)^2|V_T(r_1)-V_T(r_2)|. \tag{6.3}$$

Since the total distribution function f is broken into a series of distribution functions, the integral equation (6.1) can be broken into a sum of integrals,

$$\frac{d}{dt}N\overline{R^p}=\tfrac{1}{2}\sum_{i=1}^{I}\sum_{j=1}^{I}\Phi_{ij}^p, \tag{6.4}$$

$$\Phi_{ij}^p=\int_0^\infty\int_0^\infty F^p(r_1,r_2)V(r_1|r_2)f_i\langle r_1\rangle f_j\langle r_2\rangle dr_1dr_2. \tag{6.5}$$

The autoconversion case (i.e., $i=j$) is the most straightforward case to treat in this model. Tables of ϕ_{ii}^p are calculated for a sufficient range of $\bar{R}_i$ and σ_i^2 to be used during the cloud model calculation. The case of using two distribution functions requires the precalculation of 5 two-dimensional tables, i.e., for $p=0, 1, 2, 4, 5$. The contributions to the total moment tendencies due to the autoconversion process (i.e., a distribution interacting with itself) are then looked up in a table and renormalized by N_i^2.

The collection case (i.e., $i\neq j$) is more troublesome because table lookup techniques seem impractical because of the large number of degrees of freedom. The approach which was finally adopted for the "collection pair" tendency calculation for the log-normal set was that of fitting $F^p\cdot V(\equiv\gamma)$ to an eighth-order polynomial in x_i and x_j, as described by (5.10). The resulting approximate integral of (6.5) is then given as

$$\Phi_{ij}^p=N_iN_j\sum_{n=1}^{9}\sum_{m=1}^{9}WG_nWG_m\gamma_{nm}. \tag{6.6}$$

A stable method which was both accurate, as well as economical, was not found for the gamma distribution set for the calculation of the collection pair coalescence tendency. Thus, due to the difficulty of using this type of distribution function as a basis function for cloud physical calculations, it was finally dropped from the model.

7. Computational statistics of a double log-normal model

A single time step for two log-normal distributions requires approximately 3.15 ms when both conden-

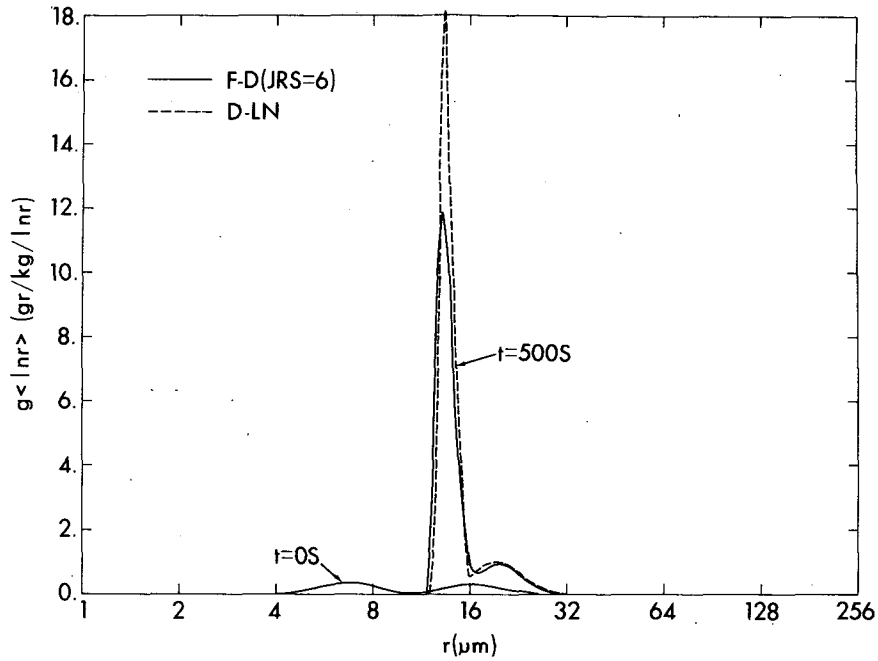

FIG. 2. Comparison of $g\langle \ln r\rangle$ vs r at $t=500$ s for case 1. The initial and final values of $g\langle \ln r\rangle$ are shown for the F-D ($JRS=6$) calculations.

sation ($K\neq 0$) and coalescence theory are considered. The CPU time required for just condensation or just coalescence theory is 1.31 ms and 2.46 ms, respectively. Thus the inclusion of stochastic coalescence theory increases the computing time by only a factor of about 2.4 over condensation alone. These statistics are for a CDC 7600 machine. Since the present code is still not fully optimized, the above figures are likely to be even further reduced. The finite-difference model calculations for $JRS=2$ were requiring about 15 ms per time step for both condensation and coalescence theory so that this method represents a significant speed-up for results (as will be presented) which are more accurate and require less than one-tenth of the field variables. Reducing the number of field variables in a cloud model is extremely important when one or more spatial dimensions are to be considered. Of course, the details on how to incorporate this type of model into Eulerian spatial domain still have to be worked out. The next section will show comparisons between the conventional finite-difference model and the present distribution model.

8. Results

The finite-difference model was initialized with the identical droplet distribution functions and thermodynamic variables as used in the distribution model. Resolution experiments were then performed for

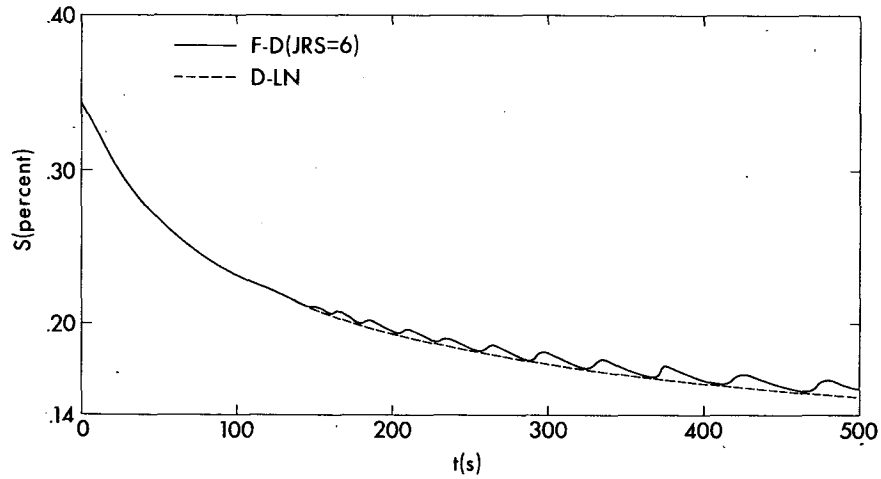

FIG. 3. Comparison of $S(t)$ vs t between F-D ($JRS=6$) for case 1.

$JRS=2, 3, 4, 5, 6$, where the length of time integration was taken as 500 s for all cases. Table 1 summarizes the main assumptions of the different cases treated. In order to gauge the accuracy of the distribution models results they will be compared with the finite-difference resolution experiments.

The initial conditions for the double distribution calculations were arbitrarily taken as

$$\left.\begin{aligned} N_1&=190\ \text{cm}^{-3}\\ N_2&=10\ \text{cm}^{-3}\\ \overline{R_1}&=6.0\ \mu\text{m}\\ \overline{R_2}&=15.0\ \mu\text{m}\\ d_1&=d_2=0.2, \end{aligned}\right\}, \tag{8.1}$$

where d_i refers to the coefficient of dispersion for the ith distribution. S was initially set equal to its quasi-steady value of approximately 0.3435%. The initial values of T and P were 10°C and 850 mb, respectively.

a. Two log-normal distributions

Figs. 1–3 show the comparison between the finite-difference model (which will subsequently be referred to as the F-D model) and the double log-normal model (the D-LN model) for case 1. Fig. 1 shows that after 500 s of integration the F-D model shows a considerable amount of dispersion for the lower resolution runs. For easier comparison with the F-D results, the absolute value of the error was plotted for the D-LN case because all errors for $p>3$ were negative. (This is the only figure where this was done.) We can see that the accuracy of the D-LN calculation is comparable to the F-D ($JRS=4$) and possibly as accurate as the F-D ($JRS=5$). As will be seen, the F-D model did not achieve a fully converged solution for even the $JRS=6$ case. At any rate, the accuracy of the six-parameter model (D-LN) is comparing well with the F-D model where more than 120 parameters were used. Fig. 2 shows the plots of $g\langle\ln r\rangle$ vs r for the F-D ($JRS=6$) and D-LN calculation at $t=500$ s. The initial distribution is also plotted for comparison. We see in this figure that the D-LN model has predicted the phases accurately but shows a considerably narrower distribution at smaller radii with a resulting higher maximum value of $g\langle\ln r\rangle$. The difference in narrowness is attributed to the D-LN models resolution for the calculation of moment tendencies being relatively insensitive to the narrowness of the particular distribution under consideration. Fig. 3 shows $S(t)$ vs t for the D-LN and F-D ($JRS=6$) calculations. The magnitude, time of onset, and frequency of the oscillations in S were found to be resolution dependent for the F-D model. They were showing clear signs of diminishing with increasing resolution. The cause of these oscillations is apparently due to the hole-filling scheme having to perform a considerable amount of work to keep $f\langle J\rangle$ positive definite. The logarithmic spacing of finite-difference grids does not seem to be appropriate for condensation theory, for the cases treated, because the limiting coefficient of dispersion is independent of radius position and, unless some broadening mechanism is imposed, the model will eventually run out of resolution. The advantage of using second-order or higher differencing schemes is that this lack of resolution often shows up as oscillations in some of the field variables, whereas the lower order schemes do not make the inadequacies of the model so apparent. The complete lack of oscillations in S for the D-LN model indicates that there are no apparent resolution problems. It is interesting that the values of S for the D-LN model are accurately fitting the lower envelope of the solution for the F-D model.

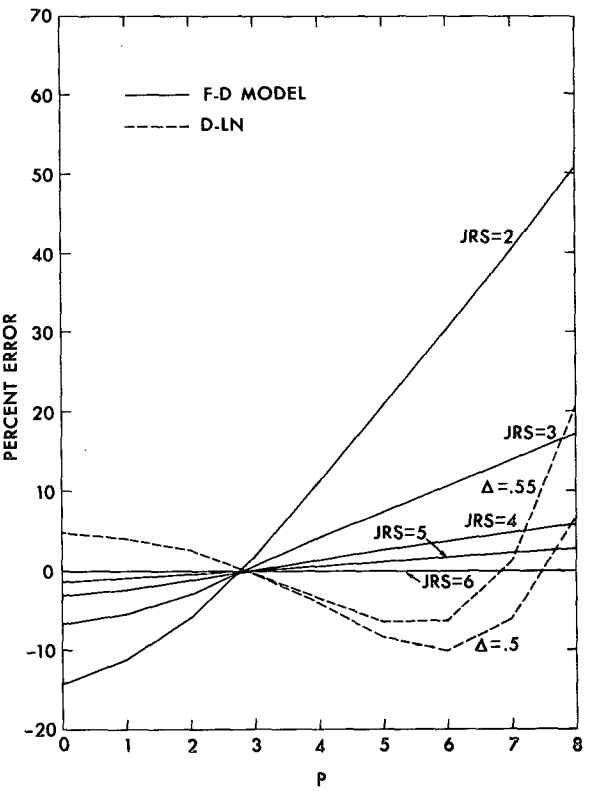

FIG. 4. As in Fig. 1 except for case 2.

Figs. 4 and 5 show comparisons between the F-D and D-LN models for case 2, where condensation theory plus the stochastic coalescence theory are considered, without any eddy mixing considered. In Fig. 4 we see that the error levels for the F-D models have considerably increased from those of case 1. The eighth total moment is over 50% too large for the $JRS=2$ case. The third moment, mass conservation, is rather accurately calculated for all of the models with little obvious correlation between overall accuracy in moment space and the accuracy of mass conservation. It is not too surprising that the coalescence equations give mass as their most accurately predicted moment, because this is the

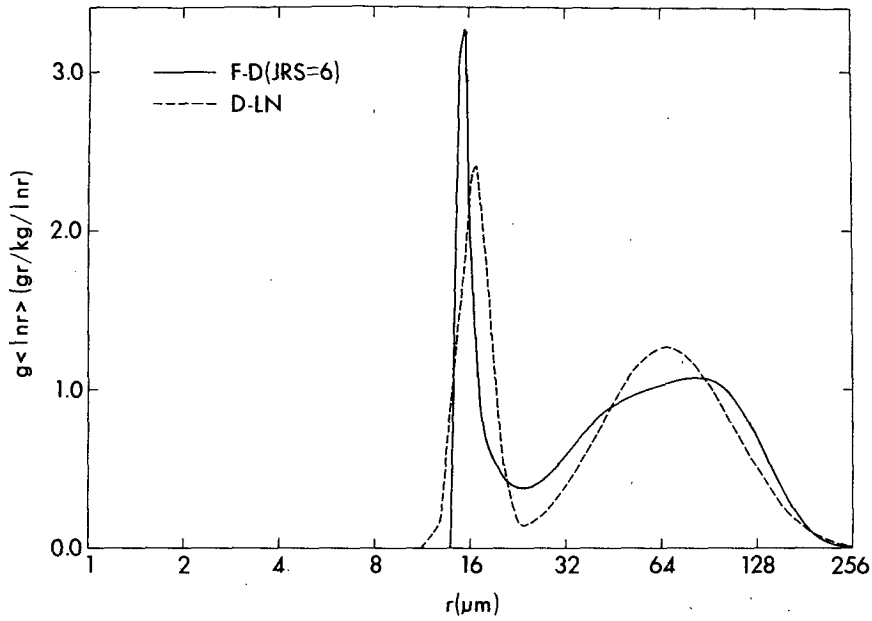

FIG. 5. As in Fig. 2 except for case 2.

only moment for which the equations are conservative. It would seem more appropriate, when referring to the accuracy of a coalescence model, to consider the slope of the error curve with respect to moment number as a measure of accuracy. Certainly this slope is not likely to be small when mass is poorly treated since mass conservation is only a necessary condition of accuracy. It is quite common in the literature to gauge a model's truncation error in terms of mass conservation when referring to the stochastic coalescence equations. For energetics the conservation of mass is clearly of fundamental importance, but it does not seem reasonable to use it as a gauge of the overall accuracy of the microphysical calculations.

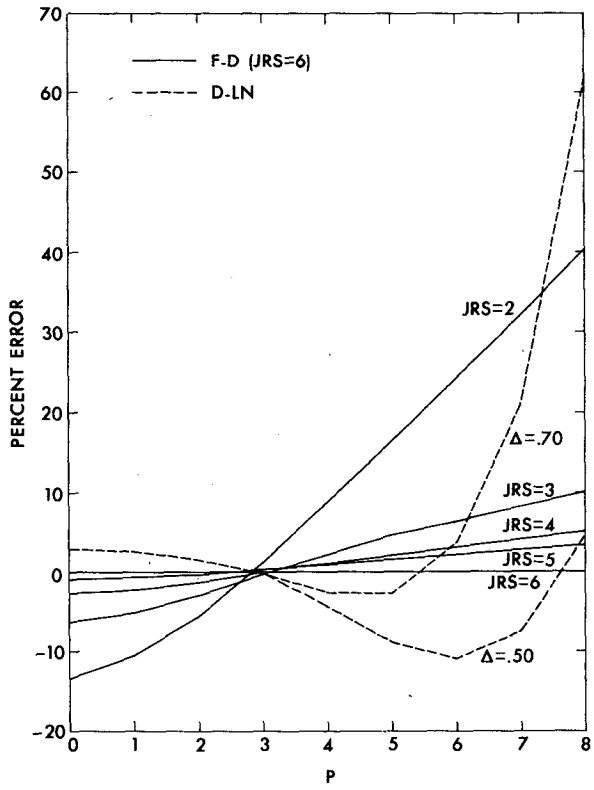

FIG. 6. As in Fig. 1 except for case 3.

The qualitative aspects of the moment error curves in Fig. 4 for the D-LN model are quite different from those of the F-D model. A continuous increase in Δ [as defined in (5.12)] from 0.5 to 0.55 was found to result in a smooth shift between the two dotted lines. Higher values of Δ are not shown because the calculations ran off the autoconversion table of tendencies. The narrowest value of σ treated by the table was 0.0495. The collection pair and condensation calculations are the only physical equations affected by this resolution parameter. Smaller values of Δ emphasize the mid-regions of the distributions, whereas larger values emphasize the tails of the distributions when calculating the approximate integration of the equations. The "best" value of Δ is found by producing a trade-off curve between noise and resolution for WG_i. As Δ is increased both resolution and "noise" decrease. Subsequent to the calculations presented in this paper $\Delta=0.58$ was found optimal. The envelope of tunable solutions for the D-LN are outperforming the $JRS=3$ calculations up to $p=5$, which is the highest moment explicitly treated by the model. The D-LN is also easily tuned to outperform the F-D ($JRS=3$) up to and including $p=8$. Fig. 5 shows plots of $g\langle \ln r\rangle$ vs r at $t=500$ s for the F-D ($JRS=6$) and D-LN ($\Delta=0.55$) models. The main

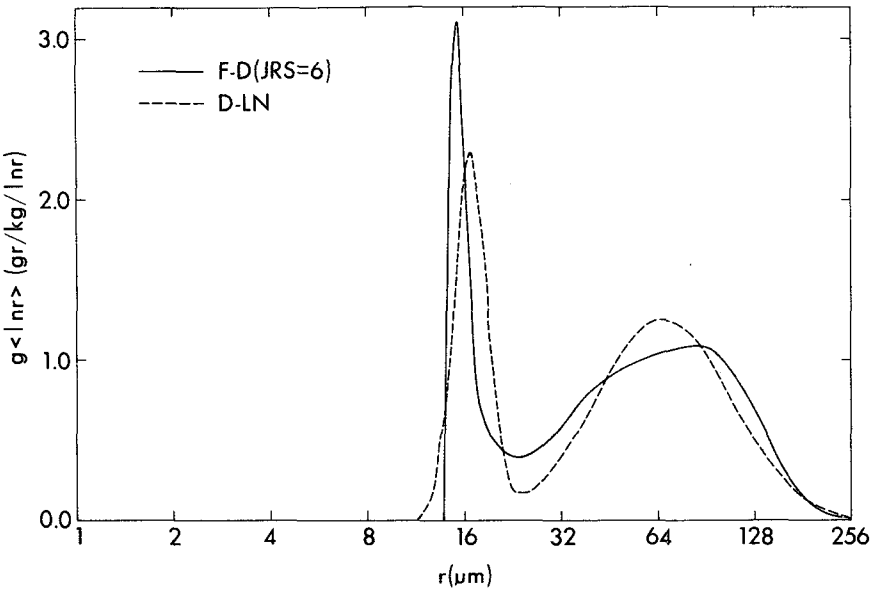

FIG. 7. As in Fig. 2 except for case 3.

differences seem to be a broader droplet spectrum predicted by the D-LN model with a resulting lower peak value and a slight "upstream" shift for the phase of the droplet distribution.

Figs. 6, 7 and 8 show comparisons between the D-LN and F-D models for case 3 where coalescence plus condensation with an eddy mixing coefficient of 4 $m^2 s^{-1}$ is considered. The main reason for including eddy mixing was to hopefully allow broader droplet distributions so that the F-D model would be able to better resolve the exact solution. There was some improvement in the level of convergence for the F-D model but it was only marginal. Just the same, it is encouraging to see the D-LN model performing as well as in the case 2 run. Figs. 6 and 7 are essentially the same as the moment error and distribution plots shown in Figs. 4 and 5, respectively. Due to the broader droplet distributions, the autoconversion table covered a sufficient range of σ, $\bar{R}$ to allow Δ to range up to 0.7. Thus in Fig. 6 we see a broader range of tunable solutions obtainable by varying Δ. In Fig. 8, we see the comparison of S vs t for the F-D ($JRS=6$) and D-LN models. The high-frequency oscillations of S (which are due to poor resolution of the droplet distribution) are again evident for the F-D

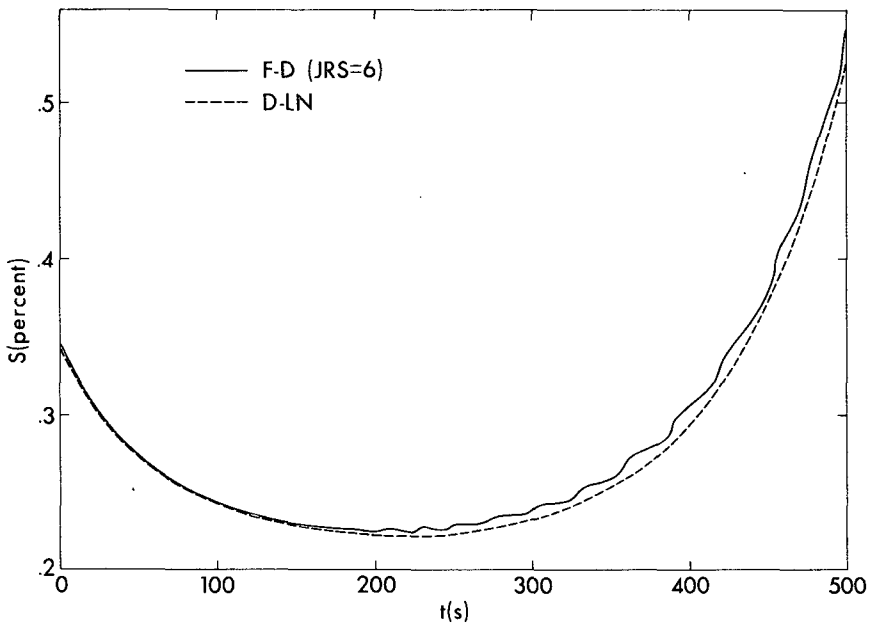

FIG. 8. Comparison of $S(t)$ vs t between F-D ($JRS=6$) and case 3.

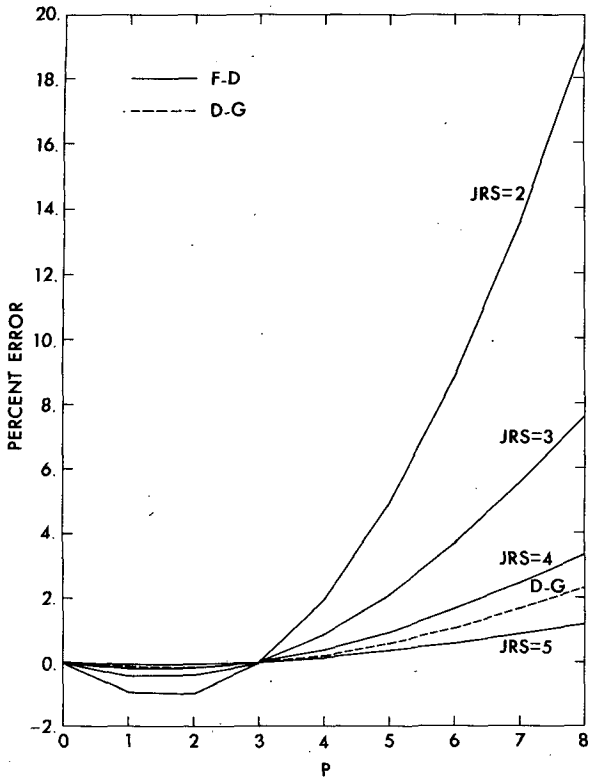

FIG. 9. As in Fig. 1 except for case 4.

model but are not present for the D-LN model. The accuracy of the D-LN model is very good for this parameter, even when S is rising due to droplet depletion through the coalescence process. It is clear that the present calculations could not be carried much further without considering renucleation. This subject is discussed by Clark (1973) and Young (1974).

b. Two gamma distributions

The author had previously used a single gamma distribution for condensation theory in Clark (1974), but in the present work, no success was achieved in trying to consider coalescence theory using gamma distributions. The only calculations to be presented are for case 4 where condensation theory with $K=4$ m^2 s^{-1} is considered. Figs. 9 and 10 show the moment error curves and comparisons of $g\langle \ln r\rangle$ at $t=500$ s, respectively. The double gamma (D-G) model has about the same error level as the D-LN model for the similar case but in this case the errors are positive. Considering the apparent lack of convergence of the F-D model, even at $JRS=6$, the negative errors of the D-LN model suggest that the log-normal distribution is better suited as a basis function for considering condensation theory. In Fig. 10, we see about the same degree of comparison of $g\langle \ln r\rangle$ between the D-G and F-D models ($JRS=6$) as there was between the D-LN and F-D models.

9. Conclusions

Calculations of condensation and coalescence theory were performed in a Lagrangian-parcel sense for a constant updraft of 2 m s^{-1}. For the identical initial conditions of two droplet distributions, the double log-normal and double gamma distribution models were compared with the solutions obtained using a conventional finite-difference model. It was found that the double log-normal model gave very accurate and computationally fast solutions for both condensation and coalescence theory. The present results indicate that using two and possibly more log-normal distributions as a set of basis functions for the cloud physical equations may be an accurate and economical method for

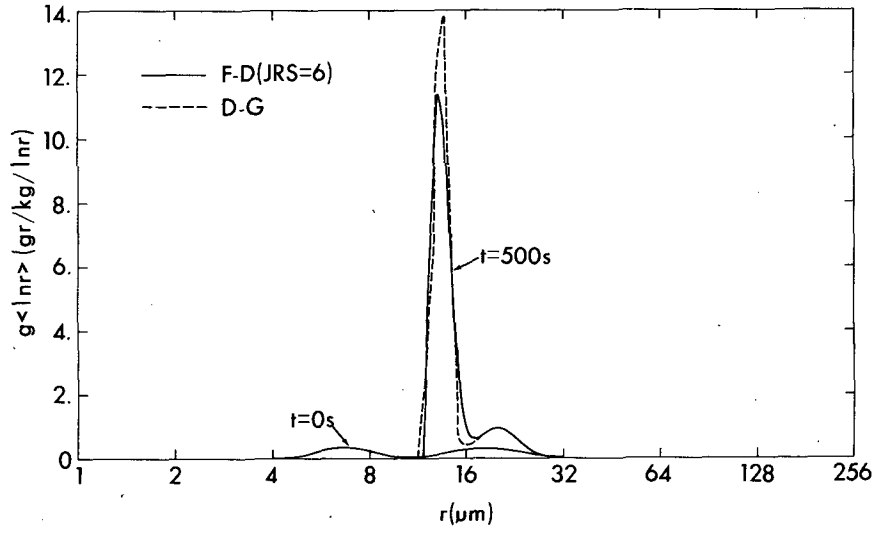

FIG. 10. As in Fig. 2 except for case 4.

consideration in dynamical as well as Lagrangian microphysical cloud models. Some particularly attractive aspects of this approach are:

1) The small number of field variables required to represent the liquid water field (the 6-parameter double log-normal model performed as accurately as a 91-parameter finite-difference model for the cases so far considered).

2) The factor of about 5 decrease in computational time for the 6-parameter log-normal model as compared with the 61-parameter finite-difference model for both condensation and stochastic coalescence theory.

3) The method of separately treating each physical process such as condensation, collection pair interaction and autoconversion could allow the development of new and useful methods of analysis leading to better understanding of the roles played by these processes (and others added in the future) in the full microphysical calculations.

The results indicate that the gamma distribution is not as suitable as the log-normal distribution function for use as a basis function when considering condensation theory. Extensive attempts were made to incorporate the gamma set into coalescence theory but these were all unsuccessful. These attempts are not presented but I should mention that when gamma distributions were used the coefficient matrix usually became singular after a short period of time integration.

The microphysical model, as presented, is still only partially developed with respect to the warm rain processes. Some further developments which seem necessary are the inclusion of nucleation, ventilation effects, curvature effects, realistic collection efficiencies and drop breakup. A numerical stability analysis which seems difficult to accomplish for this nonlinear system would certainly be useful.

Acknowledgments. The author thanks Norman McFarlane for many helpful discussions. I also appreciate the encouragement this project received from many of my colleagues.

REFERENCES

Berry, E. X, 1967: Cloud droplet growth by collection. *J. Atmos. Sci.*, **24**, 688–701.

——, and R. L. Reinhardt, 1974: An analysis of cloud drop growth by collection. *J. Atmos. Sci.*, **31**, 1814–1824.

Clark, T. L., 1973: Numerical modelling of the dynamics and microphysics of warm cumulus convection. *J. Atmos. Sci.*, **30**, 857–878.

——, 1974: On modelling nucleation and condensation theory in Eulerian spatial domain. *J. Atmos. Sci.*, **31**, 2099–2117.

Chodes, N., J. Warner and A. Gagin, 1974: A determination of the condensation coefficient of water from the growth rate of small cloud droplets. *J. Atmos. Sci.*, **31**, 1351–1367.

Drake, R. L., 1972: The scalar transport equation of coalescence theory: Moments and kernels. *J. Atmos. Sci.*, **29**, 537–547.

Long, A. B., 1974: Solutions to the droplet collection equation for polynomial kernels. *J. Atmos. Sci.*, **31**, 1040–1052.

Sedunov, Yu. S., 1974: *Physics of Drop Formation in the Atmosphere*, Wiley, 234 pp.

Thompson, P. D., 1968: A transformation of the stochastic equation for droplet coalescence. *Proc. Intern. Conf. Cloud Phys.*, Toronto, 115–126.

Young, K. C., 1974: The evolution of drop spectra through condensation, coalescence and breakup. *Preprints Conf. Cloud Physics*, Tucson, Ariz., Amer Meteor. Soc., 95–98.